Desalination and Water Treatment
www.deswater.com

doi:10.5004/dwt.2018.21921

107 (2018) 62–71
March

The catalysis biodecolorization characteristics of novel recyclable insoluble redox mediators onto magnetic nanoparticles

Caicai Lu[a], Dan Yang[a], Jianbo Guo[a,*], Zhen Xie[a], Yuanyuan Song[a], Yajuan Xing[b], Huu Hao Ngo[a], Yi Han[a], Haibo Li[a]

[a]*School of Environmental and Municipal Engineering, Tianjin Key Laboratory of Aquatic Science and Technology, Tianjin Chengjian University, Jinjing Road 26, Tianjin 300384, China, email: lucaicai2010@163.com (C. Lu), yangdan1518@163.com (D. Yang), Fax +86-22 -23085116, jianbguo@163.com (J. Guo), 1612786189@qq.com (Z. Xie), Song23735735@126.com (Y. Song), HuuHao.Ngo@uts.edu.au (H.H. Ngo), hanyi1127@126.com (Y. Han), lhb19850725@163.com (H. Li)*
[b]*Key Laboratory of Recycling and Eco-treatment of Waste Biomass of Zhejiang Province, School of Civil Engineering and Architecture, Zhejiang University of Science and Technology, Hangzhou 310023, China, email: xing_yajuan@126.com (Y. Xing)*

Received 6 September 2017; Accepted 11 January 2018

ABSTRACT

The insoluble redox mediators (RMs) were prepared to overcome limitations of soluble RMs that are eluted with water flow in wastewater treatment process. Magnetic nanoparticles possess good performance, due to their high specific surface area, the absence of internal diffusion resistance and easy separation in presence of an external magnetic field. In this study, insoluble RMs were prepared by immobilizing anthraquinone-2-sulfate (AQS) onto magnetic nanoparticles. AQS modified magnetic nanoparticles (FeSi@AQS) were formed by chemical reaction between the sulfochlorides group of anthraquinone-2-sulfonyl choride and amino-modified magnetic nanoparticles, with formation confirmed by Fourier transform infrared spectra. Results of *energy dispersive X*-ray and thermal gravimetric analysis showed that AQS occupied a 21.47 wt.% proportion of the FeSi@AQS complex. FeSi@AQS was used as insoluble RMs to catalyze biodecolorization of several kinds of azo dyes. When the concentration of FeSi@AQS was as low as 40 mg/L, biodecolorization rate of reactivered K-2BP was increased by 2.18-fold. FeSi@AQ Scan then be separated and gathered from wastewater by magnetic attraction and reused for further catalysis of azo dye decolorization in a modified SBR system. These findings show that the immobilization of RMs on magnetic nanoparticle surfaces, benefits potential industrial applications of RMs.

Keywords: Insoluble redox mediators; Magnetic nanoparticles; Separation; Catalysis biodecolorization

1. Introduction

Azo dyes are extensively applied in many industries, such as in the dyeing, textile and paper industries [1–3]. Many azo dyes and their degradation products, such asaromatic amines, are toxic to living organisms, causing mutagenic and carcinogenic effects that pose a serious public health concern [3–5]. Microbial azo dye remediation [6] has been extensively studied due to its benefits of being eco-friendly and cost-effective [7]. In these systems, microbial remediation of azo dyes occurs by anaerobic and aerobic processes [8]. In anaerobic systems dyes are first converted to aromatic a mine compounds, while further aerobic treatment generates CO_2 and inorganic compounds [9]. One notable limitation however, is that the microbial metabolism rate of azo dyes under anaerobic conditions is low, reducing the rate of azo dye bio-remediation [10,11].

In order to overcome the low anaerobic bio-reduction rate, redox mediators (RMs), (or electron shuttle) was introduced to catalyze refractory pollutant anaerobic biotransformation [9]. Previous studies have reported that RMs have been successfully employed for the catalysis of

*Corresponding author.

anaerobic bio-reduction of persistent contaminants such as azo dyes [12–15]; nitro aromatics [16,17]; halogenated pollutants [18]; and high valence heavy metals [19–23]; among others. It has been well documented that humic substances and quinone analogs [24] can behave as RMs by catalyzing transformation, accelerating the process by several orders of magnitudes [9,25].

A significant problem in practical application of RM technology, however, is that soluble RMs are eluted with water flow therefore requiring continual dosing, resulting in unrealistically high costs as well as presenting a serious secondary pollution risk [26,27]. Therefore, the potential use of insoluble/immobilized RMs has received much research interest, aiming to overcome limitations in wastewater treatment process applications. The immobilization of anthraquinone-2,6-disulfonate (AQDS) by calcium alginate [28] was reported for the first time by the author in 2007. Further studies then reported optimized or varying approaches to immobilize RMs, using carriers such as polyurethane foam [29], poly (ethylene terephthalate) fiber [30], and anion exchange resins [31]. Some disadvantages of these immobilizing techniques in practical application are the gradual loss of the redox mediating capacity due to factors such as RMs wash-out from bioreactors or disruption of immobilizing material, and mass transfer limitations due to the major fraction of the RMs remained entrapped within the immobilizing material [32]. Compared to the aforementioned traditional macro-sized carriers used for RM immobilization, nano-sized carriers have been found to have an improved performance due to their high specific surface area and the absence of internal diffusion resistance, resulting in higher catalytic efficiency [33]. Research using metal-oxide nanoparticles as adsorbents to immobilize AQDS and humic acid found that the solid-phase RMs formed, presented up to 7.5-fold increased catalytic efficiency [30,32,34]. Despite these benefits, the significant risk of run-off does however remain when using nanoparticles as a solid carrier, resulting in a significant secondary pollution risk. Therefore, it is essential to develop new techniques for RMs immobilization that limit the risk of environmental contamination.

Magnetic nanoparticles [35] have been extensively studied as environmentally functional materials, benefiting from their high specific surface area; the absence of internal diffusion resistance; and their ability to be magnetically separated and collected in the presence of an external magnetic field [36,37]. To our knowledge this is the first reported study to successfully generate an insoluble RM, by immobilizing anthraquinone-2-sulfate (AQS) onto magnetic Fe_3O_4 nanoparticles. Magnetic Fe_3O_4 nanoparticles were prepared by co precipitation of Fe^{3+} and Fe^{2+} with an amino-group then grafted to the surface of magnetic nanoparticles using a silane coupling agent. Meanwhile, AQS was modified toanthraquinone-2-sulfonyl choride (AQSCl), which was then reacted with amino-modified magnetic nanoparticles ($FeSi@NH_2$) to obtain the final AQS modified magnetic nanoparticles (FeSi@AQS). Fourier transform infrared (FT-IR), dynamic light scattering (DLS), *energy dispersive X*-ray (EDX) and thermal gravimetric analysis (TGA) were carried out to both qualitatively and quantitatively explore FeSi@AQS characteristics and properties. The catalytic effects of FeSi@AQS on the decolorization of azo dyes (e.g., reactivered K-2BP (RR 2), reactive brilliant orange X-GN; acidic golden G; reactive violet K-3R; and direct fast black G)were evaluated. In addition, FeSi@AQS was successfully separated and gathered from waste water by magnetic attraction and then reused to catalyze azo dye decolorization in a modified SBR system.

2. Methods

2.1. Materials

AQS (98% purity, Sigma Aldrich) was selected as a model RM. Triethylamine (TEA, Tianjin Chemical Co.) was purified by distillation prior to use. Tetraethyl orthosilicate (TEOS) and 3-Aminopropyltriethoxysilane (APTES, purity >99%) were purchased from Alfa Aesar. $FeCl_3{\cdot}6H_2O$, $FeCl_2{\cdot}4H_2O$ and dichloro methane were purchased from Tianjin HEOWNS Biochemical Technology Co. The azo dyes (RR 2; reactive brilliant orange X-GN; acidic golden G; reactive violet K-3R; and direct fast black G) were supplied by Dye Synthesize Laboratory, Dalian University of Technology. The basalmediu mutilized for azo dye decolorization was Luria-Bertani (LB) medium, containing 10 g/L peptone, 5 g/L yeast extract and 5 g/L NaCl. All other chemicals were of analytical reagent grade.

2.2. Preparation of FeSi@AQS

Magnetic Fe_3O_4 nanoparticles were prepared by chemical precipitation as reported in the literature [38]. Silica coated Fe_3O_4 magnetic nanoparticles ($Fe_3O_4@SiO_2$) were prepared using the Stöber method. Firstly, Fe_3O_4 (60 mg) was dispersed in a solution of water and ethanol (3:7, v: v), then TEOS (1 mL) and ammonia (7 mL) were added in a nitrogen atmosphere at room temperature. Finally, the product was repeatedly washed using ethanol and distilled water in turn. $Fe_3O_4@SiO_2$ was obtained by magnetic separation and vacuum drying. $FeSi@NH_2$ was formed using a silane coupling agent. $Fe_3O_4@SiO_2$ (100 mg) was treated with the mixture of ethanol (2 mL), APTES (0.4 mL) and an ammonia solution (1.5 mL, 25–28%) for 2 h. Nanoparticles were then rinsed with ethanol and distilled water and dried under a stream of nitrogen to obtain the $FeSi@NH_2$.

Anthraquinone sulfonyl chloride (AQSCl) was synthetized by the modification of AQS, allowing the sulfochloride group of AQSCl to react with the amino group of $FeSi@NH_2$. In detail, AQS (2.72 g) was dissolved in 150 mL methylene chloride, then chloro sulfonic acid (HSO_3Cl) (4 mL) was added to the solution in a drop wise manner and the reaction was then maintained at 40°C for 6 h. Then solution was extracted and washed three times with NaCl solution (10 *wt.*%). The organic phase was preserved and dried for 12 h to remove the water by using magnesium sulfate. Dichloro methane was removed by rotary evaporation. Finally, AQSCl was collected and dried under vacuum.

AQS modified magnetic nanoparticles were prepared by chemical reaction between AQSCl and $FeSi@NH_2$ in the presence of an acid-binding agent. Firstly, $FeSi@NH_2$ (0.118 g) were dispersed in 100 mL of chloroform, then 5 mL TEA was added, forming 'solution A'. AQSCl (0.9200 g) was dissolved in chloroform (50 mL), resulting in 'solution B'. Solution B was then added to solution A in a drop wise manner in 30 min and reacted for another 4 h. The final

FeSi@AQS was obtained using magnetic separation, then washed using ethanol and dried under vacuum at ambient temperature.

2.3. Decolorization assays of azo dye

Decolorization bacteria were prepared in-lab according to published methods [39]. During the logarithmic growth phase, the mixed solution of bacteria (10 mL) was inoculated into LB medium (200 mL). Biomass concentration was determined by optical density (OD) at 600 nm, and the relationship between the bacterial cell concentration and OD 600 nm for strain was established as 1.0 OD = 3.16 g dry cell/L.

The initial concentration of reactive red K-2BP (RR 2) in the mixture was 200 mg/L, with FeSi@AQS also combined into the solution to explore its catalytic efficiency as compared to control groups. Control-1 group (C-1) proceeded without the addition of the bacterial inoculation, while Control-2 group (C-2) was carried out without the addition of the FeSi@AQS catalyst. Experiment groups were conducted with varying FeSi@AQS concentrations: 10 mg/L (E-1 group); 20 mg/L (E-2 group) and 40 mg/L (E-3 group).

All serum bottles used for test were covered by rubber cover and aluminous model to maintain an anaerobic environment. At every 2 h interval, 5 mL sample was taken out and the concentration of RR 2 was tested. The concentrations of azo dyes were established using previously reported methods [39]. The absorbance of azo dye solution was monitored by measuring maximum absorbance at λ = 534 nm and the concentration of azo dye were established based on standard curve data. All assays were performed in triplicate and the mean values of the data are presented. The decolorization of azo dye was calculate according to formula (1):

$$\text{Decolorization efficiency (\%)} = (C_0 - C_t)/C_0 \times 100\% \quad (1)$$

where C_0 is the initial concentration of azo dye, C_t is the concentration of azo dye at t time.

In addition to RR2, several other azo dyes were investigated to assess the catalytic effect of FeSi@AQS nanoparticles, namely: reactive brilliant orange X-GN; acidic golden G; reactive violet K-3R and direct fast black G. In all cases experimental procedures were as outlined for RR2.

2.4. Separation and reutilization of FeSi@AQS

Separation and reutilization of FeSi@AQS was assessed at both bottle level and bioreactor level. In bottle level systems, a magnet was used to attract FeSi@AQS following azo dye decolorization. The collected FeSi@AQS was reused to catalyze the decolorization of azo dye ten consecutive times. Concurrently, a modified sequencing batch reactor (SBR) system was designed and operated. The modified SBR system run in five phases: Influent phase (I); reacting phase (II); precipitation phase (III); effluent phase (IV); andinact phase (V). Electromagnets were used to provide a changeable magnetic field, where during influent and reacting phases, the electromagnet was inactive, allowing FeSi@AQS to disperse in solution and catalyze the decolorization of azo dyes. Conversely, in the effluent phase the electro magnet was active and attracted FeSi@AQS nanoparticles, avoiding wash-out of RM with effluent flow.

2.5. Analysis method

FT-IR spectra of FeSi@NH_2, AQS and FeSi@AQS were established using an FT-IR spectrometer model FTS 6000 spectrophotometer (BIO-RAD, USA) at room temperature. Samples were prepared by well dispersing the complex in KBr powder, then compressing mixtures to form a plate. A total of 64 scans were performed at a resolution of 4 cm^{-1}. Thermogravimetric analysis (TGA) used to investigate nanoparticle stability under a nitrogen atmosphere with heating rate of 10°C min^{-1}. TGA was performed out using a Rheometric Scientific TGA1500 (Piscataway, NJ) to assess thermal properties of samples. The chemical compositions of FeSi@NH_2 and FeSi@AQS were identified by EDX. The hydrodynamic size of nanoparticles was analyzed by Dynamic light scattering (DLS) using a Zetasizer Nano ZS90 (Malvern Instruments, South borough, MA), with a fixed scattering angle of 90° and measurements recorded at a constant temperature (25°C) in triplicate. The oxidation reduction potential (ORP) and pH were measured usingan ORP combine delectrode (501, INESA Scientific Instrument Co, Ltd) and a pH meter (METTLER TOLEDO FE 20).

3. Results and discussion

3.1. Immobilization of AQS on Fe_3O_4 magnetic nanoparticles

Magnetic nanoparticles possess good performance, due to their high specific surface area, the absence of internal diffusion resistance and easy separation in presence of an external magnetic field [40]. In the present study, Fe_3O_4 magnetic nanoparticles were used as the biocarrier of AQS, with Fig. 1b illustrating the process of immobilization of AQS on to the surface of Fe_3O_4. Magnetic nanoparticles were synthesized by co precipitation of Fe^{2+} and Fe^{3+}, with the addition of ammonia. Furthermore, as Fe_3O_4 nanoparticles show high sensitivity to oxygen, silica is commonly used as a coating, forming stable magnetic nanoparticles [41]. Additionally, the silica shell can passivate the surface of magnetic nanoparticles during or following synthesis, avoid particle agglomeration. In this study, Fe_3O_4 nanoparticles were coated with a silica shell as per the Stöber method, forming Fe_3O_4@SiO_2 nanoparticles. Amino-modified magnetic nanoparticles FeSi@NH_2 were prepared using the silane coupling agent, 3-Aminopropyltriethoxysilane (APTES), which was covalently bound to the surface of Fe_3O_4@SiO_2 nanoparticles. Amino-modification brought reactive functional groups to nanoparticle surfaces, which make subsequent AQS reactions feasible.

Anthraquinone sulfochlorides (AQSCl) was synthetized by the modification of AQS as shown in Fig. 1a, where the AQS sulfo group was converted to a sulfo chloride by reaction with HSO_3Cl. The AQSCl sulfo chlorides group can then react with the amino group of FeSi@NH_2 in the presence of an acid-binding agent. As a result, AQS was immobilized onto the surface of magnetic nanoparticles by chemical interaction, forming FeSi@AQS.

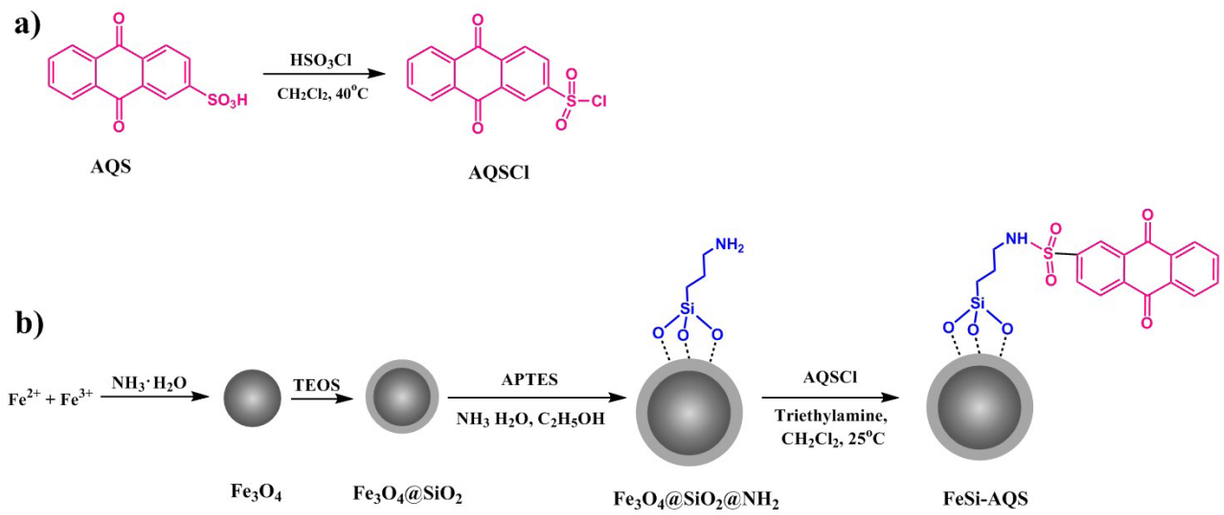

Fig. 1. (a) Synthesis of AQSCl. (b) The immobilization of AQS on the surface of Fe_3O_4magnetic nanoparticles.

3.2. Characterization of FeSi@AQS

FeSi@AQS and its intermediate products were characterized by FT-IR, DLS, TEM, EDX and TGA, to qualitatively and quantitatively explore their compositions, structures and other properties. To confirm reactions and the formations of chemical linkages between AQS and magnetic nanoparticles, FT-IR spectroscopy was used to establish FT-IR spectra for FeSi@NH_2 (Fig. 2A); AQS (Fig. 2B); and FeSi@AQS (Fig. 2C). As shown in Fig. 2B, the weak band visible at 1678 cm^{-1} and the band visible at approximately 1585.3 cm^{-1}, can be attributed to carbonyl group (C=O) stretching vibrations in anthraquin one. The bands visible at 960 cm^{-1} and 928 cm^{-1} were assigned as bending vibrations of the (S-O) bond. As shown in Fig. 2C, the characteristic spectral signals for both carbonyl (C=O) and sulfonate (SO^{3-}) groups were visible at 1700–1630 cm^{-1} and 1290–1100 cm^{-1}, respectively. As shown by FT-IR results, the FeSi@AQS spectrum showed characteristic absorption bands corresponding to AQS, confirming that Fe_3O_4 was successfully modified by AQS during the reaction.

The hydrodynamic diameters and zeta potentials of both FeSi@AQS and their intermediate products, were investigated using DLS and as shown in Figs. 3a–d, the hydrodynamic diameters of Fe_3O_4, Fe_3O_4@SiO_2, FeSi@NH_2 and FeSi@AQS were 69 nm, 148 nm, 162 nm and 166 nm, respectively. The modification of $Fe_3O_4$with silica was shown to increase the hydrodynamic diameter, partly due to the additional volume occupied by silica on the outer sphere of Fe_3O_4, as well as due to agglomeration of Fe_3O_4 nanoparticles [41]. Conversely, further amino-modification of AQS nanoparticles resulted in only a marginal change in observed hydrodynamic diameters.

The zeta potentials of Fe_3O_4, Fe_3O_4@SiO_2, FeSi@NH_2 and FeSi@AQS are presented in Fig. 3e showing the zeta potential of Fe_3O_4 and Fe_3O_4@SiO_2 to be –32 mV and –29 mV, respectively. The surface of Fe_3O_4 was found to contain abundant hydroxyl groups, generating negatively charged oxygen ions by ionization. The zeta potential changed from negative to positive, following APTES modification, due to binding of the amino group and a hydrogen proton, forming ammonium which provides the nanoparticle with an overall positive charge. However, following reaction of the AQSCl sulfo chlorides group with nanoparticle amino groups, the degree of positive charge decreased significantly. The final nanoparticles showed only minor levels of negative charge, confirming that most amino groups had reacted with the sulfo chloride group of AQSCl. All hydrodynamic diameter and zeta potential data support and confirm the reactions outlined in Fig. 1b.

Quantitative characterization of AQS bound on nanoparticle surfaces was performed by TGA and EDX and as shown in Fig. S2. The weight loss tendencies of FeSi@NH_2 (Fig. S2A) and FeSi@AQS (Fig. S2B) established with rising temperatures from 25 to 800°C. The weight loss observed below 200°C generally corresponds to the loss of water, in both free and bound form, while the organic compounds, such as APTES and AQS, convert to a gas composition at temperatures of above 200°C. Based on TGA curves established, the weight losses for FeSi@NH_2 and FeSi@AQS in the range of 200–800°C, were 19.20% and 41.96%, respectively. In comparison with the TGA curve established for FeSi@NH_2 (Fig. S2A), the additionally loss of weight observed in curve B can be attributed to AQS, with a loss of 22.76%. Therefore, the grafting weight ratio of AQS on the surface of nanoparticles was established to be 22.76%.

The elemental composition of FeSi@AQS was verified by EDX analysis, with elemental analysis showing that FeSi@AQS contained 2.29 *wt.*% S and 1.55 *wt.*% H. Elemental compositions were calculate according to formula (2):

$$\text{AQS } wt.\% = \text{S } wt.\% \times Mr_{(AQS)}/Mr_{(S)} \quad (2)$$

where $Mr_{(S)}$ represents the formula weight of the Satom (32 g/mol); $Mr_{(AQS)}$represents the molecular weight of AQS (272 g/mol). According to formula (1), the amount of AQS bound on FeSi@AQS was 19.47 wt.%. It is of note, that data obtained by TGA measurements and those calculated based on EDX results presented only minor differences,

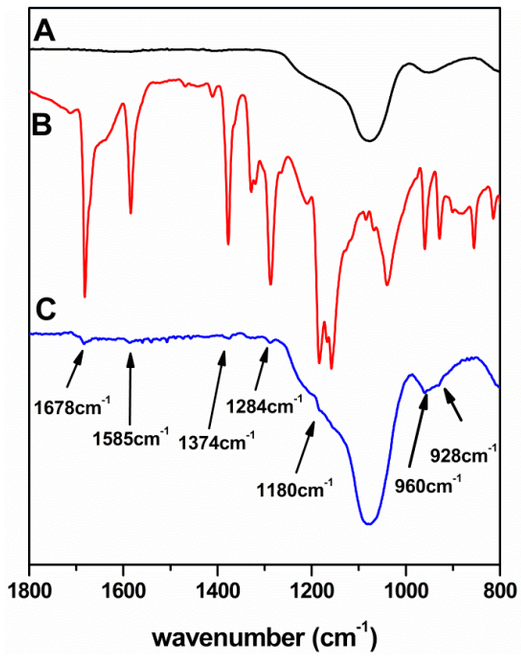

Fig. 2. FT-IR spectra of FeSi@NH_2 (A), AQS (B) and FeSi@AQS (C).

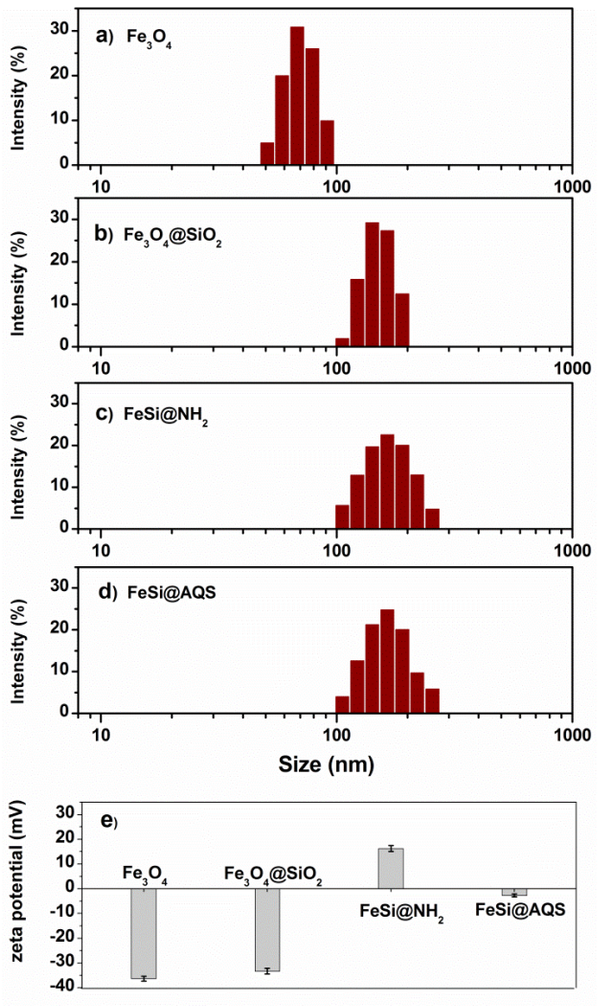

Fig. 3. Hydrodynamic diameters and distribution of Fe_3O_4 (a); Fe_3O_4@SiO_2 (b); FeSi@NH_2 (c); and FeSi@AQS nanoparticles (d); and their zeta potential at pH 7 (e).

which may be due to methodological differences. Mean values of the results obtained by EDX and TGA analysis were used to quantify the AQS portions of FeSi@AQS, showing its relative abundance to be 21.12 wt.%, translating to 0.78 m mol AQS per 1 g FeSi@AQS nanoparticle matter. Compared with findings from previously reported literature with other RM carriers, magnetic nanoparticles are shown to possess a high loading efficiency, due to their high specific surface area which supports a high catalytic efficiency.

3.3. Biodecolorization of azo dye

The catalytic properties of FeSi@AQS were evaluated by assessing the decolorization of the azo model compound, RR2, a stable and persistent azo compound commonly used to represent reductive decolorization processes in textile wastewater treatment systems [42]. Fig. 4a shows the effects of the presence of FeSi@AQS on the decolorization of RR2, as compared to control-1 group (C-1) which did not contain any bacterial inoculation. During the 12 h experimental period, no significant decolorization (<2.0%) of RR2 was observed, suggesting that physical-chemical processes such as adsorption or chemical reduction were not responsible for the enhanced level of decolorization achieved. The molar concentration of immobilized AQS used in incubations were 7.8 μmol/L, 15.6 μmol/L and 31.2 μmol/L, respectively. Compared with control group (C-2), which was conducted without any FeSi@AQS catalyst, it is obvious that FeSi@AQS clearly accelerates the decolorization of RR2 in a concentration dependent manner, FeSi@AQS increasing azo compound decolorization in the E-1 group by 1.38-fold; in the E-2 group by 1.80-fold; and in the E-3 by 2.18-fold.

Besides RR2, several other azo dyes, reactive brilliant orange X-GN, acidic golden G, reactive violet K-3R, direct fast black G were also used to investigate the catalytic effect of FeSi@AQS nanoparticles. As shown in Fig. 4b, the biodecolorization rate of reactive brilliant orange X-GN, acidic golden G, reactive violet K-3R, direct fast black G was increased by 1.2-fold, 1.16-fold,1.51-fold, 1.25-fold, respectively. The results show that FeSi@AQS was efficient in treatment of various azo dyes.

Fig. 5 shows ORP data, with changes visible due to the decolorization of RR 2, where reduction of the azo dye to aromatic a mine, causes a decrease of ORP. When comparing to control groups, in Group E and Group A, a higher decolorization efficiency was observed in the presence of both FeSi@AQS and AQS. The initial redox potentials of both Group E and Group A were higher than that of the control group. During the entire process of azo dye decolorization, significant increase in ORP observed for FeSi@AQS, at approximately 20 mV higher than that of the con-

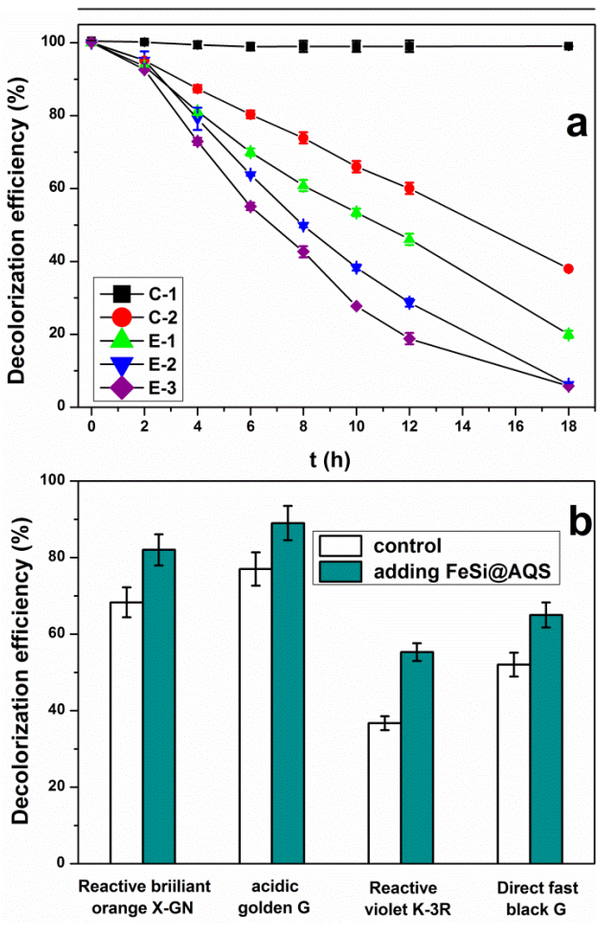

Fig. 4. (a) Decolorization of RR2 with varying conditions. Control-1 group (C-1) proceed without adding any consortium bacteria. While none FeSi-AQS was added in Control-2 group (C-2). Experiment groups were carried with different concentrations of FeSi@AQS, which was 10 mg/L (E-1 group), 20 mg/L (E-2 group) and 40 mg/L (E-3 group), respectively. (b) four kinds of azo dye (reactive brilliant orange X-GN, acidic golden G, reactive violet K-3R, direct fast black G) were used to compare their catalytic efficiency to FeSi@AQS. The concentration of azo dye remaining was tested following 8 h reaction time.

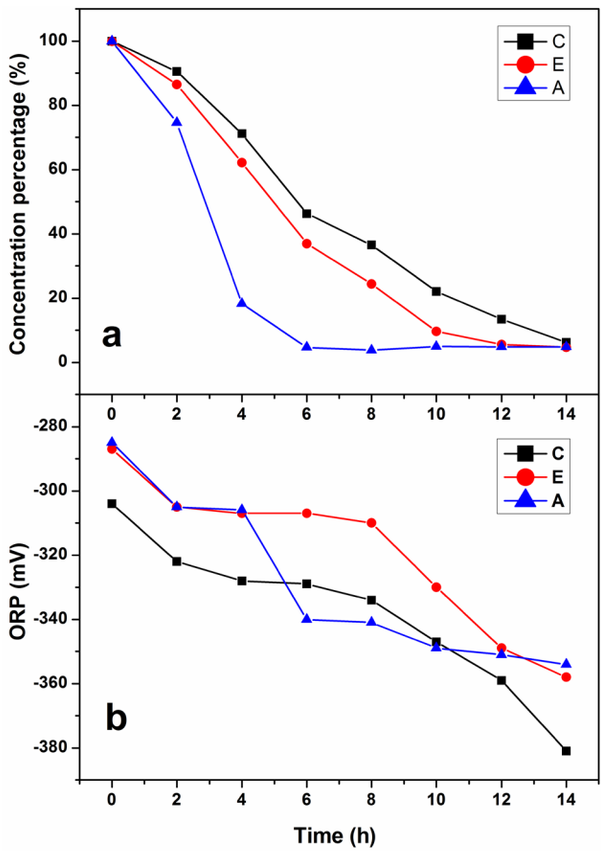

Fig. 5. Decolorization of RR2 under varying catalytic conditions (a) and the corresponding ORP of solution during RR2 decolorization (b). Control analysis (Group C) was performed without any RMs, while experimental group E contained FeSi@AQS (10 mg/L); and experimental group A contained 10 mg/L AQS. C, E, A in the figure are the data of Group C, Experimental group E and Experimental group A, respectively.

trol. These findings provide supportive evidence that the FeSi@AQS decolorization system FeSi@AQS represents a less reductive environment, which is more suitable for the effective decolorization of azo dyes.

3.4. Separation and reutilization of FeSi@AQS in bottle and bioreactor level systems

In order to investigate the recovery and reutilization of the obtained FeSi@AQS, a magnet and an electromagnet were used to separate FeSi@AQS from wastewater. Fig. 6a–c show the magnetic separation of by magnetic separation in sample bottle. In dispersed solutions, nanoparticles were rapidly collected toward a magnet placed on the outer surface of reagent bottles, causing the dark dispersion (Fig. 6a) became clear (Fig. 6b). When the magnetic field was removed, the collected particles were re-dispersed into solution (Fig. 6c) by ultrasonic dispersion. These findings indicate that magnetic nanoparticles can easily be manipulated by an external magnetic field, which is of great significance for the separation and recovery of RMs during practical application processes.

Following biodecolorization of RR2, FeSi@AQS was separated from wastewater by magnetic separation, with FeSi@AQS nanoparticles gathered and reused for 6 cycles of biodecolorization. The initial loading concentration of FeSi@AQS was 40.0 mg and following 6 usage cycles, 33.7 mg was recovered, showing a recovery level of 80.8%. Fig. 6d show the FeSi@AQS catalytic effect on RR2 biodecolorization for 6 cycles in a bottle level. As cycle numbers increased, the catalytic efficiency slightly decreased, which is likely due to the loss of FeSi@AQS present in the system due to the process of separation and sampling. Overall, these results show that the catalytic efficiency of FeSi@AQS nanoparticles did not significantly reduce according to increasing cycle numbers, suggesting that FeSi@AQS can serve as an effective insoluble RM.

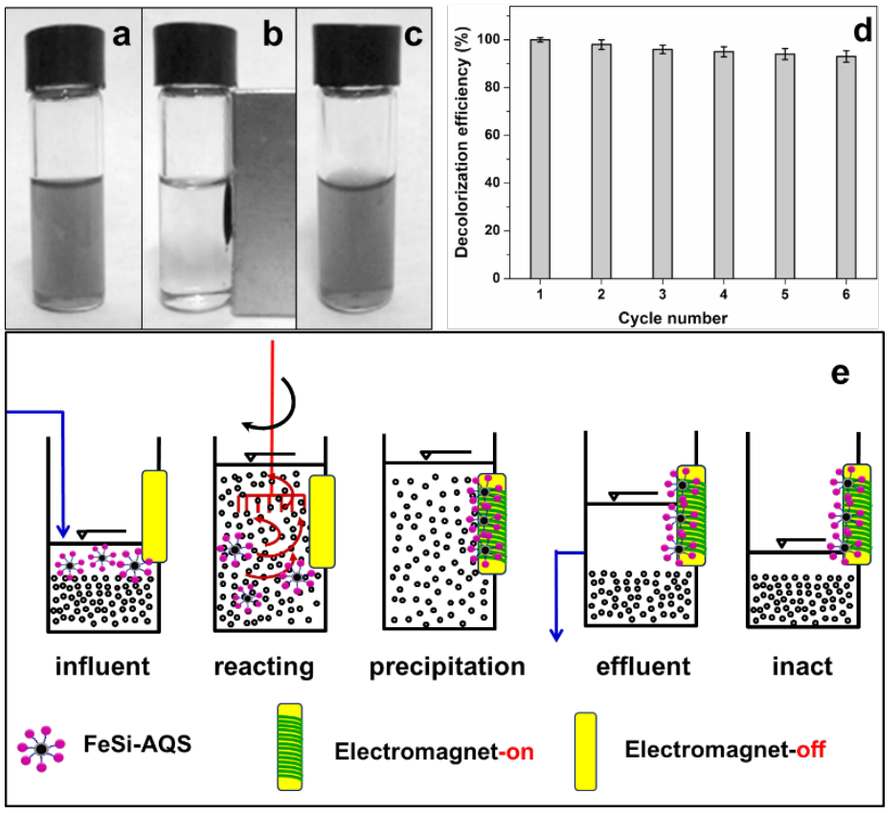

Fig. 6. Photographs of the FeSi@AQS dispersed in aqueous solution static condition (a), after the application of a localized magnetic field (b) and re-dispersion after removing the magnetic field (c). FeSi@AQS catalytic effect on the biodecolorization of RR2, with 6 repeated cycles in a bottle level(d). FeSi@AQS was used in a modified SBR system (e).

Sequencing batch reactor (SBR) systems are wastewater treatment processes that have a large potential range of application. In the present study, a modified SBR system was designed and operated as shown in Fig. 6e, with an electromagnet used to provide a changeable magnetic field. The modified SBR system run in five phase: Influent phase (I), reacting phase (II), precitation phase (III), effluent phase (IV) and in act phase (V). During phase III, IV and V, the electromagnet remained active, resulting in FeSi@AQS being adsorbed to the surface of the electromagnet, avoiding the loss of RM with effluent run-off. Conversely, during influent and reacting phases (phase I and II), the electromagnet was inactive, allowing the FeSi@AQS to disperse in solution with stirring, further catalyzing the decolorization of azo dyes. These findings indicate that magnetic nanoparticles can easily be manipulated by an external magnetic field, which is of great significance for the separation and recovery of RMs during practical application processes.

Previous studies have reported various approaches to the application of RMs to catalyze refractory pollutant anaerobic biotransformation. A notable disadvantage of these immobilizing techni0ques in practical application is the gradual loss of redox mediating capacity due to either wash-out of the RMs from bioreactors, or due to disruption of immobilizing material, limiting mass transfer due to the major fraction being entrapped within the immobilizing material [32]. In the present study, AQS was investigated as a model RM and immobilized on magnetic Fe_3O_4 nanoparticles by chemical interaction. Other RMs can also immobilize on magnetic Fe_3O_4 nanoparticles, with using specific corresponding silane coupling agents. As compared to the traditional supports used in RM immobilization processes, several advantages exist for the use of magnetic nanoparticles as an immobilizing material. Firstly, magnetic nanoparticles possess a relatively good catalytic performance due to their high specific surface area and the absence of mass transfer limitations; secondly, the high surface area of magnetic nanoparticles results a larger capacity to immobilize RM; and thirdly, magnetic nanoparticles have the ability to be separated magnetically, and then reused. Overall, magnetic nanoparticles are of great potential in the immobilization and practical application of RMs.

4. Conclusion

In this study, an insoluble RM, FeSi@AQS, was prepared by immobilizing AQS on the surface of magnetic Fe_3O_4 nanoparticles by chemical interaction. FT-IR analysis confirmed the chemical reaction between AQSCl and FeSi@NH_2. EDX and TGA analysis established that the proportion of AQS bound to the surface of FeSi@AQS is 21.47 wt.%. When the molar concentration of immobilized AQS used in incubations was 31.2 μmol/L, biodecolorization rate of RR 2

was increased by 2.18-fold. FeSi@AQS effectively catalyzed the biological decolorization of RR2 and four other azo dyes, due to the generation of a less reductive environment by FeSi@AQS. Further benefits exist as FeSi@AQS can then be separated and be collected from wastewater effluent by magnetic attraction, allowing reuse to further catalyze the azo dye decolorization in a modified SBR system. These findings show that FeSi@AQS nanoparticles offer high catalytic activity, magnetic separability and good long-term stability, supporting their potential use in industrial application.

Acknowledgements

This study was supported by the National Natural Science Foundation of China (Grant No. 51678387 and Grant No.51708389) and Key project of Tianjin Natural Science Foundation (17JCZDJC39300).

References

[1] A. Shimizu, M. Tokumura, K. Nakajima, Y. Kawase, Phenol removal using zero-valent iron powder in the presence of dissolved oxygen: Roles of decomposition by the Fenton reaction and adsorption/precipitation, J. Hazrd. Mater., 201 (2012) 60–67.

[2] S. Sansuk, S. Srijaranai, S. Srijaranai, A new approach for removing anionic organic dyes from wastewater based on electro statically driven assembly, Environ. Sci. Technol., 50 (2016) 6477–6484.

[3] W.F. Khalik, S.-A. Ong, L.-N. Ho, Y.-S. Wong, N.A. Yusoff, F. Ridwan, Evaluation on the molecular structure of azo dye in photo catalytic mineralization under solar light irradiation, Desal. Water Treat., 55 (2015) 2229–2236.

[4] P.V. Nidheesh, R. Gandhimathi, S.T. Ramesh, Degradation of dyes from aqueous solution by Fenton processes: a review, Environ. Sci. Pollut. R., 20 (2013) 2099–2132.

[5] A. Thiam, I. Sires, E. Brillas, Treatment of a mixture of food color additives (E122, E124 and E129) in different water matrices by UVA and solar photo electro-Fenton, Water Res., 81 (2015) 178–187.

[6] U. Kalsoom, H.N. Bhatti, M. Asgher, Characterization of plant peroxidases and their potential for degradation of dyes: a review, Appl. Biochem. Biotech., 176 (2015) 1529–1550.

[7] R. Khan, P. Bhawana, M.H. Fulekar, Microbial decolorization and degradation of synthetic dyes: a review, Rev. Environ. Sci. Biol., 12 (2013) 75–97.

[8] N. Dafale, S. Wate, S. Meshram, N.R. Neti, Bioremediation of wastewater containing azo dyes through sequential anaerobic-aerobic bioreactor system and its biodiversity, Environ. Rev., 18 (2010) 21–36.

[9] F.R. Van der Zee, F.J. Cervantes, Impact and application of electron shuttles on the redox (bio) transformation of contaminants: A review, Biotechnol. Adv., 27 (2009) 256–277.

[10] A. Colunga, J.R. Rangel-Mendez, L.B. Celis, F.J. Cervantes, Graphene oxide as electron shuttle for increased redox conversion of contaminants under methanogenic and sulfate-reducing conditions, Bioresour. Technol., 175 (2015) 309–314.

[11] E.J. O'Loughlin, Effects of electron transfer mediators on the bioreduction of lepidocrocite (gamma-FeOOH) by Shewanella putrefaciens CN32, Environ. Sci. Technol., 42 (2008) 6876–6882.

[12] F.P. van der Zee, S. Villaverde, Combined anaerobic-aerobic treatment of azo dyes - A short review of bioreactor studies, Water Res., 39 (2005) 1425–1440.

[13] Y. Mu, K. Rabaey, R.A. Rozendal, Z.G. Yuan, J. Keller, Decolorization of azo dyes in bioelectro chemical systems, Environ. Sci. Technol., 43 (2009) 5137–5143.

[14] S. Sreelatha, G. Velvizhi, A.N. Kumar, S.V. Mohan, Functional behavior of bio-electro chemical treatment system with increasing azo dye concentrations: Synergistic interactions of biocatalyst and electrode assembly, Bioresour. Technol., 213 (2016) 11–20.

[15] A. Aris, K. Muda, M.R. Salim, Z. Ibrahim, COD and color removal from textile effluent using granular sludge biomass: effect of substrate and riboflavin, Desal. Water Treat., 52 (2014) 7366–7376.

[16] C. Aranda-Tamaura, M.I. Estrada-Alvarado, A.C. Texier, F. Cuervo, J. Gomez, F.J. Cervantes, Effects of different quinoid redox mediators on the removal of sulphide and nitrate via denitrification, Chemosphere, 69 (2007) 1722–1727.

[17] Z.X. Xiao, T. Awata, D.D. Zhang, C.F. Zhang, Z.L. Li, A. Katayama, Enhanced denitrification of Pseudomonas stutzeri by a bioelectro chemical system assisted with solid-phase humin, J. Biosci. Bioeng., 122 (2016) 85–91.

[18] F. Aulenta, V. Di Maio, T. Ferri, M. Majone, The humic acid analogue antraquinone-2,6-disulfonate (AQDS) serves as an electron shuttle in the electricity-driven microbial dechlorination of trichloroethene to cis-dichloroethene, Bioresour Technol., 101 (2010) 9728–9733.

[19] A. Ramos-Ruiz, J.A. Field, J.V. Wilkening, R. Sierra-Alvarez, Recovery of elemental tellurium nanoparticles by the reduction of tellurium oxyanions in a methanogenic microbial consortium, Environ. Sci. Technol., 50 (2016) 1492–1500.

[20] L.A. Liu, Y. Yuan, F.B. Li, C.H. Feng, In-situ Cr(VI) reduction with electro generated hydrogen peroxide driven by iron-reducing bacteria, Bioresour. Technol., 102 (2011) 2468–2473.

[21] B. Shan, Y.Z. Cai, J.D. Brooks, H. Corke, Antibacterial properties and major bioactive components of cinnamon stick (Cinnamomum burmannii): Activity against foodborne pathogenic bacteria, J. Agr. Food Chem., 55 (2007) 5484–5490.

[22] B. Kavita, H. Keharia, Anthraquinone 2-sulfonic acid-mediated reduction of Cr(VI) by Bacillus sp. BT1, Desal. Water Treat., 53 (2015) 221–229.

[23] J. Huang, M. Wu, J. Tang, R. Zhou, J. Chen, W. Han, Z. Xie, Enhanced bio-reduction of hexavalent chromium by an anaerobic consortium using henna plant biomass as electron donor and redox mediator, Desal. Water Treat., 57 (2016) 15125–15132.

[24] S. Qiao, T. Tian, J.T. Zhou, Effects of quinoid redox mediators on the activity of anammox biomass, Bioresour. Technol., 152 (2014) 116–123.

[25] A. Keck, J. Klein, M. Kudlich, A. Stolz, H.J. Knackmuss, R. Mattes, Reduction of azo dyes by redox mediators originating in the naphthalene sulfonic acid degradation pathway of Sphingomonas sp. strain BN6, Appl. Environ. Microb., 63 (1997) 3684–3690.

[26] J.B. Guo, L. Kang, J.L. Yang, X.L. Wang, J. Lian, H.B. Li, Y.K. Guo, Y.Y. Wang, Study on a novel non-dissolved redox mediator catalyzing biological denitrification (RMBDN) technology, Bioresour. Technol., 101 (2010) 4238–4241.

[27] R.B. Dai, X.G. Chen, C.Y. Ma, X.Y. Xiang, G. Li, Insoluble/immobilized redox mediators for catalyzing anaerobic bio-reduction of contaminants, Rev. Environ. Sci. Biol., 15 (2016) 379–409.

[28] J.B. Guo, J.T. Zhou, D. Wang, C.P. Tian, P. Wang, M.S. Uddin, H. Yu, Biocalalyst effects of immobilized anthraquin one on the anaerobic reduction of azo dyes by the salt-tolerant bacteria, Water Res., 41 (2007) 426–432.

[29] H. Lu, J.T. Zhou, J. Wang, W.L. Si, H. Teng, G.F. Liu, Enhanced biodecolorization of azo dyes by anthraquinone-2-sulfonate immobilized covalently in polyurethane foam, Bioresour. Technol., 101 (2010) 7185–7188.

[30] Q. Xu, J.B. Guo, C.M. Niu, J. Lian, Z.H. Hou, Y.K. Guo, S.Y. Li, The denitrification characteristics of novel functional biocarriers immobilised by non-dissolved redox mediators, Biochem. Eng. J., 95 (2015) 98–103.

[31] F.J. Cervantes, A. Garcia-Espinosa, M. Antonieta Moreno-Reynosa, J.R. Rangel-Mendez, Immobilized redox mediators on anion exchange resins and their role on the reductive

decolorization of azo dyes, Environ. Sci. Technol., 44 (2010) 1747–1753.
[32] L.H. Alvarez, M.A. Perez-Cruz, J.R. Rangel-Mendez, F.J. Cervantes, Immobilized redox mediator on metal-oxides nanoparticles and its catalytic effect in a reductive decolorization process, J. Hazard. Mater., 184 (2010) 268–272.
[33] R.M. Kakhki, Application of magnetic nanoparticles modified with cyclodextrins as efficient adsorbents in separation systems, J. Incl. Phenom. Macro., 82 (2015) 301–310.
[34] F.J. Cervantes, R. Gomez, L.H. Alvarez, C.M. Martinez, V. Hernandez-Montoya, Efficient anaerobic treatment of synthetic textile wastewater in a UASB reactor with granular sludge enriched with humic acids supported on alumina nanoparticles, Biodegradation, 26 (2015) 289–298.
[35] S. Fathi Karkan, M. Mohammadhosseini, Y. Panahi, M. Milani, N. Zarghami, A. Akbarzadeh, E. Abasi, A. Hosseini, S. Davaran, Magnetic nanoparticles in cancer diagnosis and treatment: a review, Artif. Cell. Nanomed. B., 45 (2017) 1–5.
[36] J.-F. Liu, Z.-S. Zhao, G.-B. Jiang, Coating Fe_3O_4 magnetic nanoparticles with humic acid for high efficient removal of heavy metals in water, Environ. Sci. Technol., 42 (2008) 6949–6954.
[37] C.T. Yavuz, J.T. Mayo, W.W. Yu, A. Prakash, J.C. Falkner, S. Yean, L. Cong, H.J. Shipley, A. Kan, M. Tomson, D. Natelson, V.L. Colvin, Low-field magnetic separation of mono disperse Fe_3O_4 nano crystals, Science, 314 (2006) 964–967.
[38] S. Wu, A. Sun, F. Zhai, J. Wang, W. Xu, Q. Zhang, A.A. Volinsky, Fe_3O_4 magnetic nanoparticles synthesis from tailings by ultrasonic chemical co-precipitation, Mater. Lett., 65 (2011) 1882–1884.
[39] J.B. Guo, H.J. Liu, J.H. Qua, J. Lian, L.J. Zhao, W. Jefferson, J.L. Yang, The structure activity relationship of non-dissolved redox mediators during azo dye bio-decolorization processes. Bioresour. Technol., 112 (2012) 350–354.
[40] X. Qu, P.J.J. Alvarez, Q. Li, Applications of nano technology in water and wastewater treatment, Water Res., 47 (2013) 3931–3946.
[41] P. Xu, G.M. Zeng, D.L. Huang, C.L. Feng, S. Hu, M.H. Zhao, C. Lai, Z. Wei, C. Huang, G.X. Xie, Z.F. Liu, Use of iron oxide nano materials in wastewater treatment: A review, Sci. Total Environ., 424 (2012) 1–10.
[42] J.M. Wu, W. Wen, Catalyzed degradation of azo dyes under ambient conditions, Environ. Sci. Technol., 44 (2010) 9123–9127.

Supporting information

Transmission Electron Microscopy (TEM). The morphology of nanogels was characterized by TEM. The digital images were recorded on a JEOL microscope (Japan). A specimen suspension under different conditions was prepared as below: a drop of the suspension was placed onto a 200 mesh copper grid, and then dried at the corresponding temperature in a vacuum drying chamber for preparing TEM samples.

TEM was used to observe the morphology of Fe_3O_4. The TEM images are shown in Fig. S2. Being consistent with the DLS data, TEM images indicated a very good dispersion of nanoparticles as individual spherical particles. What's more, the size of the nanogel is around 150 nm in diameter, a little smaller than that got by DLS. The slight decrease of the size is caused by the collapse of the hydration layer on the surface of the nanogel particles.

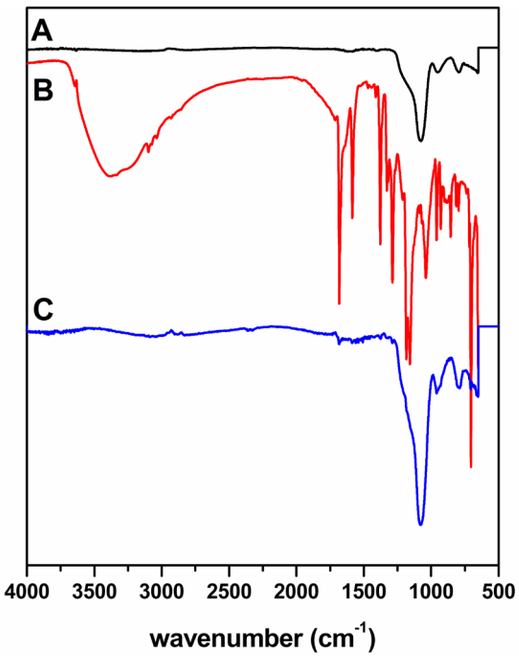

Fig. S1. FT-IR spectra of $FeSi@NH_2$ (A), AQS (B) and FeSi@AQS (C).

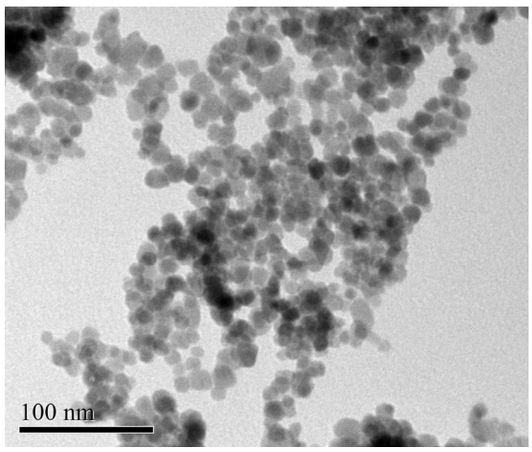

Fig. S2. TEM images of Fe_3O_4.

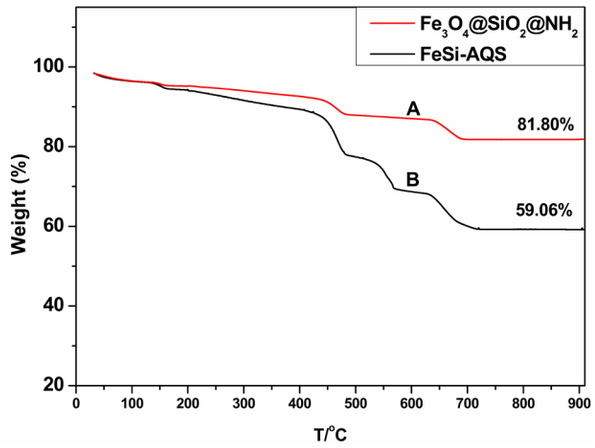

Fig. S3. Weight loss of $FeSi@NH_2$ (A) and FeSi@AQS (B) with increase in temperature from 25 to 800 °C.